CrossMark

RESEARCH PAPER

Nitrile-functionalized ruthenium nanoparticles: charge delocalization through Ru − N ≡ C interface

Fengqi Zhang · Lin Huang · Jiasui Zou · Jinwu Yan ·
Jiaying Zhu · Xiongwu Kang ⓘ · Shaowei Chen

Abstract Ruthenium nanoparticles (2.06 ± 0.46 nm in diameter) were stabilized by the self-assembly of nitrile molecules onto the ruthenium colloid surface by virtue of the formation of Ru−N≡C interfacial bonding linkages. Thermogravimetric analysis showed that there were about 63 nitrile ligands per nanoparticle, corresponding to an average molecular footprint of 22.4 Å^2. Proton nuclear magnetic resonance (NMR) studies suggested an end-on configuration of the nitrile moiety on the metal core surface. Meanwhile, infrared measurements showed that the C≡N stretch red-shifted from 2246 to 1944 cm^{-1} upon adsorption on the nanoparticle surfaces, as confirmed by ^{15}N isotopic labeling. This apparent red-shift suggests extensive intraparticle charge delocalization, which was further manifested by photoluminescence measurements of 1-cyanopyrene-functionalized ruthenium nanoparticles that exhibited a red shift of 40 nm of the emission maximum, in comparison to that of free monomers. The results further highlight the significance of metal−organic contacts in the manipulation of the dynamics of intraparticle charge transfer and the nanoparticle optical and electronic properties.

Keywords Ruthenium nanoparticles · Nitrile · Metal-organic interfacial bond · Intraparticle charge delocalization

F. Zhang · L. Huang · J. Zou · X. Kang (✉) · S. Chen (✉)
New Energy Research Institute, School of Environment and Energy, Guangzhou Higher Education Mega Centre, South China University of Technology, Guangzhou 510006, China
e-mail: esxkang@scut.edu.cn
e-mail: shaowei@ucsc.edu

J. Yan · J. Zhu
School of Bioscience and Bioengineering, Guangzhou Higher Education Mega Centre, South China University of Technology, Guangzhou 510006, China

S. Chen
Department of Chemistry and Biochemistry, University of California, 1156 High Street, Santa Cruz, CA 95064, USA

Introduction

Metal nanoparticles capped with organic monolayers exhibit unique optical and electronic properties and have found diverse applications in, for instance, molecular electronics, chemical sensing, and catalysis (Lu and Chen 2012; Zhao et al. 2012). It has been recognized that the nanoparticle material properties can be readily manipulated by the chemical nature of the core metal, the organic capping ligands as well as the metal-organic interfacial bonds (Hu et al. 2016b; Kang et al. 2010). In early studies, mercapto derivatives have been used as the ligands of choice for surface passivation of metal nanoparticles due to the strong affinity of thiol groups to transition metal surfaces (Chen et al. 1998). Recent studies have shown that other metal-organic bonds may exhibit more interesting chemistry, leading to further and more deliberate surface functionalization of the metal nanoparticles. Among these, formation of metal-carbon (Chen et al. 2008; Chen

et al. 2010b; Kang et al. 2012b) and metal-nitrogen (Kang et al. 2012a) covalent bonds has been demonstrated as an effective tool in the regulation of the optical and electronic properties of metal nanoparticles (Chen et al. 2008; Chen et al. 2011; Chen et al. 2010a; Chen et al. 2010b; Chen et al. 2009; Kang et al. 2012b). For instance, intraparticle charge delocalization has been observed with ruthenium nanoparticles functionalized with conjugated metal-carbon bonds, such as ruthenium-carbene (Ru = C) π bonds, ruthenium-vinylidene (Ru = C = CH–) bonds (Chen et al. 2008; Chen et al. 2009) and ruthenium-nitrene (Ru = N) bonds (Kang et al. 2012a), where the electrochemical and spectroscopic characteristics of the nanoparticle-bound organic ligands are analogous to those of their dimeric counterparts with a conjugated spacer.

Nitrile derivatives possess a terminal C ≡ N moiety that is known to readily adsorb on transition-metal surfaces, analogous to n-alkynes (Oranskaya et al. 1970a; Oranskaya et al. 1970b; Oranskaya et al. 1976; Roev et al. 1958; Tretyakov and Filimonov 1973). The exact interfacial bonding modes vary with the metal substrates and typically involve end-on or side-on interfacial bonding configurations (Leow et al. 2012; Oranskaya et al. 1976; Steiner et al. 1992). The formation of such interfacial bonds is generally accounted for by the donation of the nitrogen lone-pair electrons to the metal d orbitals which leads to an increase of the C ≡ N vibrational frequency, and concurrently electrons from the metal substrate may back-donate to the vacant π^* orbital of the nitrile group and decrease the vibrational energy (Oranskaya and Filimonov 1970; Oranskaya et al. 1976). Such unique chemistry may be exploited for the deliberate manipulation of nanoparticle surface functionalization. This is the primary motivation of the present study.

Herein, we prepared stable nitrile-functionalized ruthenium nanoparticles by the self-assembly of nitrile ligands on "bare" ruthenium colloid surfaces. Spectroscopic studies based on isotopic ^{15}N labeling suggested that the nitrile ligands adopted the end-on configuration on the nanoparticle surface. Interestingly, a significant redshift of the emission was observed with ruthenium nanoparticles capped with 1-cyanopyrene, in comparison with the free monomers, suggesting rather effective intraparticle charge delocalization between the particle-bound pyrene moieties. To the best of our knowledge, this is the first of its kind.

Experimental section

Chemicals

Ruthenium chloride (RuCl$_3$, 99%, ACROS), 1,2-propanediol (99%+, ACROS), sodium acetate (NaOAc•3H$_2$O, 99.5%, ACROS), 1-dodecanenitrile (NC12, 98%, Alfa Aesar), 1-pyrenecarboxaldehyde (98%, Energy), 1-ethynylpyrene (EPy, 96%, Alfa Aesar), hydroxylamine hydrochloride-^{15}N (98%, TRC), dodecyl aldehyde (97%, Energy), hydroxylamine hydrochloride, zinc oxide, potassium iodide, acetonitrile, and sodium thiosulfate were used as received. All solvents were obtained from typical commercial sources at their highest purity and used without further treatment. Water was supplied by a Barnstead Nanopure water system (18.3 MΩ cm).

Synthesis of 1-dodecanenitrile-^{15}N (^{15}NC12)

^{15}NC12 was synthesized by following a protocol reported previously (Kivrak and Zora 2007). In a typical synthesis, dodecyl aldehyde (1.374 mL, 6.0 mmol), hydroxylamine hydrochloride-^{15}N (542 mg, 7.8 mmol), ZnO (488 mg, 6 mmol), and KI (996 mg, 6 mmol) were dissolved in 50 mL of acetonitrile. The reaction mixture was stirred for 2.5 h at 80 °C before being cooled down to room temperature. Twelve milliliters of a 5% Na$_2$O$_3$S$_2$ aqueous solution was then added into the reaction mixture, which was stirred gently for 20 min. Acetonitrile was then removed under reduced pressure, and 100 mL of ethyl acetate was added to the remaining aqueous phase for extraction. The organic phase were collected and washed with water (2 × 100 mL) and dried over MgSO$_4$. Solvents were then removed under reduced pressure to yield purified dodecanenitrile-^{15}N as a dark yellow oil, which was denoted as ^{15}NC12.

Synthesis of 1-cyanopyrene (NPy)

NPy was synthesized by following a protocol reported in the literature (Kivrak and Zora 2007). In brief, 1-pyrenecarboxaldehyde (0.69 g, 3.0 mmol), hydroxylamine hydrochloride (271 mg, 3.9 mmol), ZnO (244 mg, 3 mmol), and KI (498 mg, 3 mmol) were dissolved in 25 mL of acetonitrile at 82 °C for 2.5 h. After the solution was cooled down to room temperature, 12 mL of a 5% Na$_2$O$_3$S$_2$ aqueous solution was added into the reaction mixture, which was stirred

gently for 20 min, and acetonitrile was removed under reduced pressure by rotary evaporation. The aqueous phase was extracted with ethyl acetate (100 mL). The organic phase was washed with water (2×100 mL) and dried over $MgSO_4$. Solvents were then removed under reduced pressure to yield purified 1-cyanopyrene as yellow particles.

Synthesis of 1,4-di(pyren-1-yl)buta-1,3-diyne (di-EPy)

Di-EPy was prepared by following a protocol reported earlier (Uptmoor et al. 2015; Yin et al. 2009). In brief, tetramethylethylenediamine (41.4 µL, 276 µmol, 20 mol%) and triethylamine (574 µL, 4.14 mmol, 3.0 eq) were dispersed in THF (2.6 mL), into which were then added EPy (325 mg, 1.38 mmol, 1.0 eq), $NiCl_2 \cdot 6H_2O$ (17.1 mg, 69.1 µmol, 5 mol%), and copper iodide (13.2 mg, 69.1 µmol, 5 mol%). The mixture was stirred at room temperature for 20 h, before the solvent was removed under reduced pressure. The crude product was purified by recrystallization, affording purified di-EPy as a light yellow solid. Mass spectrometric measurements (Fig. S1) showed three peaks at m/z = 451.1, 452.1, and 453.1, consistent with the theoretical values of the di-EPy molecules with varied isotopic combinations of H and C. The structure was further confirmed by Fourier transform infrared spectroscopy (FTIR) (Fig. S2) and NMR (Fig. S3) measurements.

Preparation of ruthenium nanoparticles

The synthetic procedure of organically capped ruthenium nanoparticles involved the preparation of ruthenium colloids by thermolysis of $RuCl_3$ in 1,2-propanediol and self-assembly of organic ligands on the ruthenium nanoparticle surface (Scheme 1), as detailed previously (Chen et al. 2006). Briefly, 0.28 mmol of $RuCl_3$ and 2 mmol of NaOAc were co-dissolved in 100 mL of 1,2-propanediol, and the solution was heated to 165 °C and thermally refluxed for 30 min under vigorous stirring. The appearance of a dark brown solution signified the formation of ruthenium nanoparticles passivated by sodium acetate. The average diameter of the nanoparticles was 2.06 ± 0.46 nm, as determined by TEM measurements (Fig. S4). Once the ruthenium nanoparticle solution was cooled down to 60 °C, 0.84 mmol of NC12 in 50 mL of toluene was added into the solution. After vigorous mixing for 3 h, a dark brown color was transferred from 1,2-propanediol to toluene, indicating the

successful passivation of ruthenium nanoparticles with organic ligands. The toluene phase was collected, and the solvents were removed by rotary evaporation. By adding copious amount of methanol into small amount of nanoparticle solution in toluene and centrifugation, the nanoparticles were precipitated, and the supernatant were discarded. Upon repeating this process for multiple times, the unbound organic ligands were removed. The resulting nanoparticles were denoted as RuNC12. Ruthenium nanoparticles passivated by [15]NC12 were prepared in a similar fashion and referred to as Ru[15]NC12.

To prepare ruthenium nanoparticles functionalized with 1-cyanopyrene or 1-ethynylpyrene, a mixture of 0.56 mmol NC12 and 0.28 mmol NPy or EPy in 50 mL of toluene was added into the ruthenium colloid solution in 1,2-propanediol for passivation and extraction. The resulting nanoparticles were denoted as RuNPy and RuEPy, respectively.

Characterization

^{1}H NMR spectroscopic measurements were carried out by using concentrated solutions of the nanoparticles in $CDCl_3$ with a Bruker 400 MHz NMR spectrometer. Photoluminescence measurements were conducted with a Horiba fluorescence spectrometer. FTIR measurements were carried out with a Nicolet FTIR spectrometer, where the samples were prepared by dropcasting the particle solutions onto a KBr disk. Thermogravimetric analysis (TGA) was performed with a METTLER instrument at a heating rate of 10 °C/min under a nitrogen atmosphere. X-ray photoelectron spectroscopic (XPS) data were acquired with a PHI 5400 instrument.

Results and discussion

The RuNC12 nanoparticles were first characterized by ^{1}H NMR measurements. From Fig. 1, one can see that in comparison to the sharp peaks observed for the free monomer (top curve), the RuNC12 nanoparticles (bottom curve) exhibited only three broad peaks at 0.89, 1.2, and 2.3 ppm, which were assigned to the terminal methyl, methylene protons of the hydrocarbon chains, and α–CH_2 protons next to the $C \equiv N$ moiety, respectively. This suggests that the nitrile ligands were indeed successfully bound on the ruthenium nanoparticle surface, as peak broadening is a spectral feature characteristic of

RuCl₃ →[1,2-propanediol / Δ, 165 °C]→ **Ru** →[1-dodecanitrile]→ **Ru**—N≡C—C₁₁H₂₃
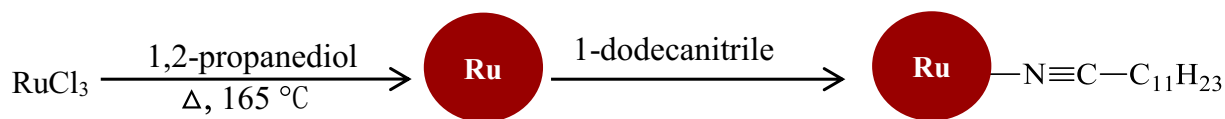
Scheme 1 Preparation of RuNC12 nanoparticles

nanoparticle-bound organic ligands, as a result of slow tumbling of the nanoparticles and diverse binding sites on the nanoparticle surfaces (e.g., vertices and terraces) (Chen et al. 2006; Hostetler et al. 1998). Interestingly, the peak at 2.3 ppm from α–CH₂ protons remained well-resolved, though markedly broadened. This suggests that the nitrile ligands most likely adopted the end-on mode on the nanoparticle surfaces (Scheme 1) (Michelin et al. 1996; Steiner et al. 1992), such that the α–CH₂ groups were situated away from the metal core, in contrast to the side-on mode where the α–CH₂ protons would be too close to the metal core and broadened into baseline (Hostetler et al. 1998).

The coverage of the nitrile ligands on the nanoparticle surface was then quantified by TGA measurements. Figure 2 depicts the TGA curve of the RuNC12 nanoparticles, which exhibited two major weight losses centered at 282 and 444 °C, as manifested in the derivative curve in the figure inset. The first weight loss of 17% commenced at about 145 °C and ended at around 370 °C, likely due to the removal of the aliphatic fragments by the breakage of the CH₂–CN bond. A less pronounced weight loss of 6% occurred at higher temperatures from ca. 410 to 520 °C, most likely due to the

removal of the C ≡ N moieties in the form of N₂ (Shanahan and Muettertiest 1984). From the weight losses, it was estimated that there were 63 nitrile ligands per nanoparticle, corresponding to a molecular footprint of 22.4 Å², which is similar to that of acetylene-functionalized ruthenium nanoparticles of similar size (Kang and Chen 2012). This is also consistent with the end-on configuration of the metal-ligand interfacial bonds, as suggested by NMR measurements (Fig. 1).

FTIR (Griffiths 2007) studies were then carried out to further examine the interaction of the nitrile group with ruthenium nanoparticle surfaces. From Fig. 3, one can see that the C ≡ N stretch appeared at 2246 cm⁻¹ for the NC12 monomers (black dashed curve), and red-shifted by 28 to 2218 cm⁻¹ for ¹⁵NC12 (dashed red curve), consistent with the isotopic mass change.

Upon adsorption of the nitrile ligands on the ruthenium nanoparticle surfaces, this sharp vibrational band disappeared; concurrently and a new vibrational band appeared at 1944 cm⁻¹ for RuNC12 (solid black curve) and 1920 cm⁻¹ for Ru¹⁵NC12 (solid red curve), as shown in the inset of Fig. 3. This might be ascribed to the nanoparticle-bound C ≡ N bonds where the red-shift, as compared to the free monomers, arose from

Fig. 1 ¹H NMR of (*top*) NC12 monomers and (*bottom*) RuNC12 nanoparticles in CDCl₃
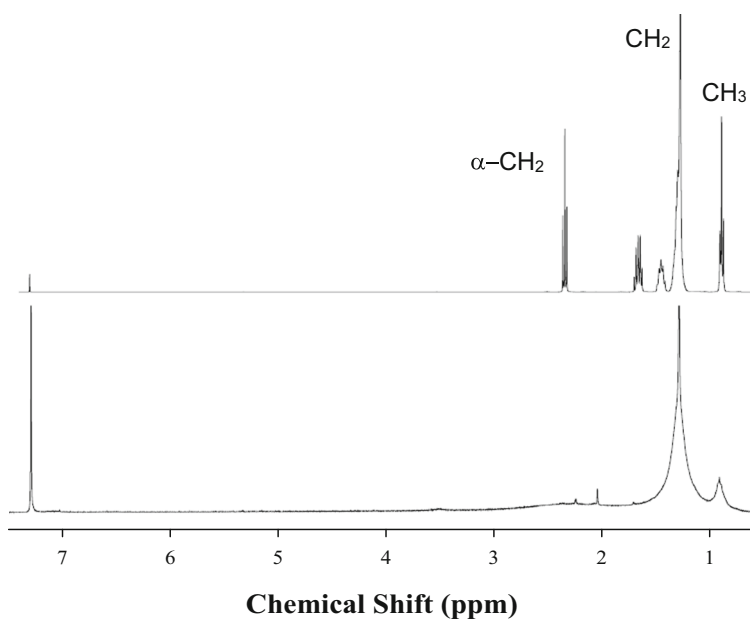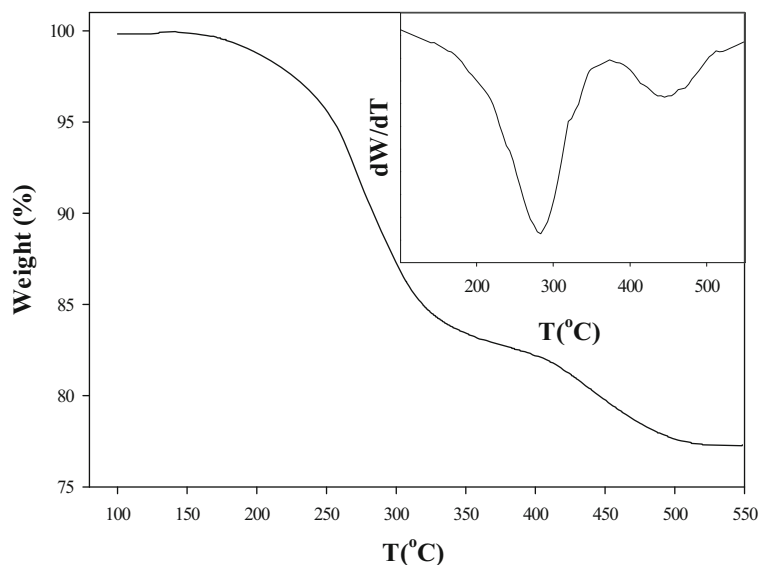
Fig. 2 TGA curve of RuNC12 nanoparticles and the inset is the first order derivative of the weight loss over temperature


intraparticle charge delocalization due to reduced metal-ligand interfacial resistance, akin to alkyne-capped nanoparticles (Michelin et al. 1996).

The bonding interactions between the nitrile moieties and the ruthenium nanoparticles were further examined by XPS measurements. Figure 4a depicts the spectrum within the range of 278 and 290 eV, where the peak (dark yellow curve) at 280.7 eV may be assigned to the $3d_{5/2}$ electrons of metallic ruthenium, with the corresponding $3d_{5/2}$ peak resolved by deconvolution at 284.9 eV (blue curve). Note that these binding energies

are 0.5–0.6 eV higher than those of bulk ruthenium (Chakroune et al. 2005; Luque et al. 2009) and 0.25 eV higher than that observed with Ru nanoparticles capped with n-alkynes (Kang and Chen 2012). The remaining two peaks at 284.7 eV (magenta curve) and 284.5 eV (cyan curve) may be assigned to sp^3 and sp. hybridized C 1 s electrons, almost identical to those of the nitrile monomers (Fig. S5).

Figure 4b depicts the high-resolution scans of the N 1 s electrons in NC12 and RuNC12 nanoparticles. One can see that both the NC12 ligands and RuNC12

Fig. 3 FTIR spectra of NC12 (*dashed black curve*), ^{15}NC12 (*dashed red curve*), RuNC12 (*solid black curve*), and Ru^{15}NC12 nanoparticles (*solid red curve*). The inset is the zoom in for the absorption band of C ≡ N bond of RuNC12 and Ru^{15}NC12 nanoparticles
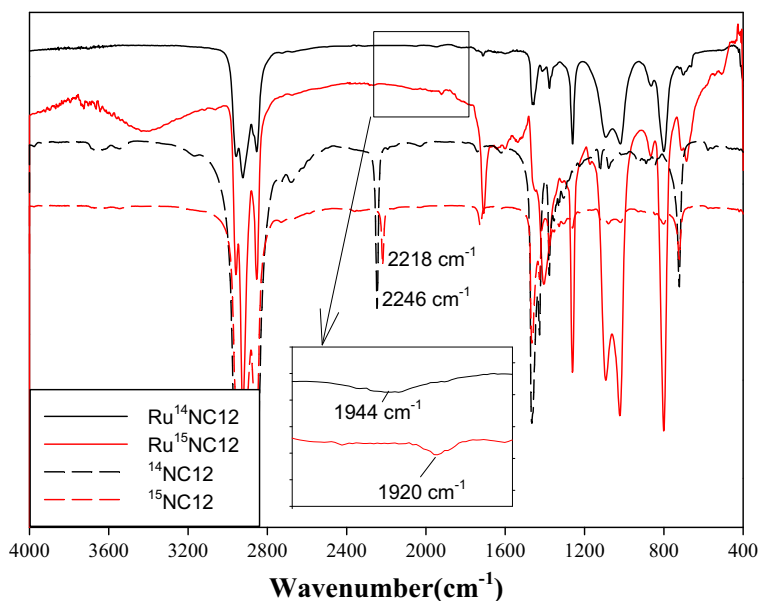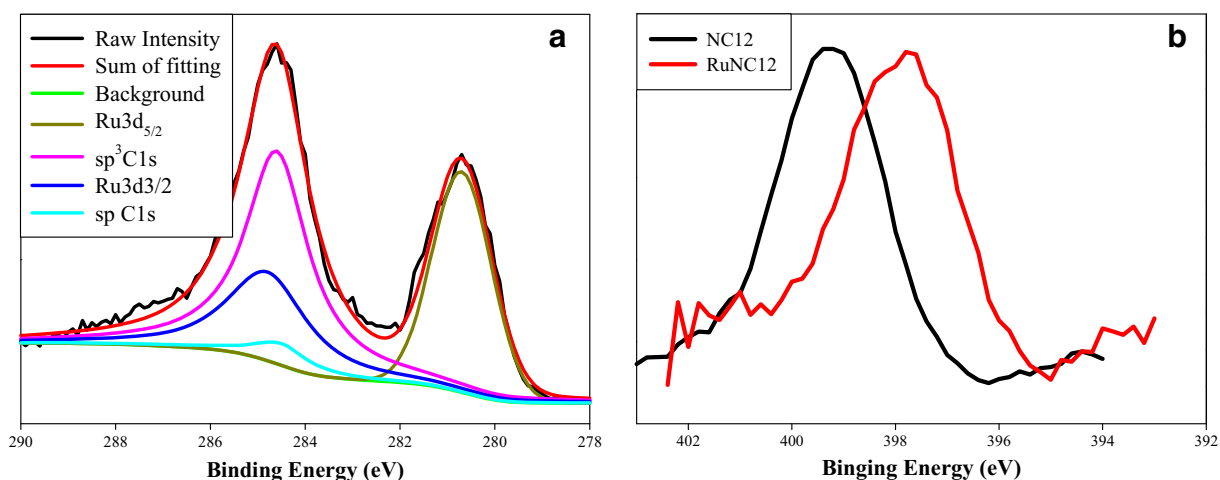
Fig. 4 High-resolution XPS scans and deconvolution of **a** Ru3d and C1s and **b** N1 s electrons in RuNC12 nanoparticles. *Black curves* are experimental data and *colored curves* are deconvolution fits

nanoparticles exhibit a single peak (Downs and Tyler 2015), yet the binding energy was markedly higher for the free ligands (399.3 eV) than for RuNC12 (397.7 eV). Such a negative shift (1.6 eV) of the N 1 s binding energy, in conjunction with the positive shift of the Ru 3d binding energy observed above, suggests an effective electron transfer from the ruthenium metal cores to the nitrile moieties at the metal-ligand interface. That is, the interfacial bonding interaction is likely dominated by d electrons from the Ru metal core back-donated to the π^* orbitals of $C \equiv N$, rather than the donation of the N lone-pair electrons to Ru. Similar behaviors have also been observed with nitrile

adsorption on transition-metal surfaces. For instance, when 1-heptadecanenitrile was adsorbed on copper, the N 1 s binding energy was found at 397.5 eV, 1.8 eV lower than that of the nitrile monomers; concurrently, the binding energy of Cu $2p_{3/2}$ electrons increased by 0.1 to 932.5 eV, relative to 932.4 eV of bulk copper (Steiner et al. 1992).

The formation of $Ru - N \equiv C$ interfacial bonds may then be exploited for the manipulation of nanoparticle optical and electronic properties. This is demonstrated with RuNPy nanoparticles. Figure 5 depicts the excitation and emission spectra of the NPy monomer and RuNPy nanoparticles in CHCl₃.

Fig. 5 Excitation and emission spectra of NPy monomers and RuNPy nanoparticles in chloroform
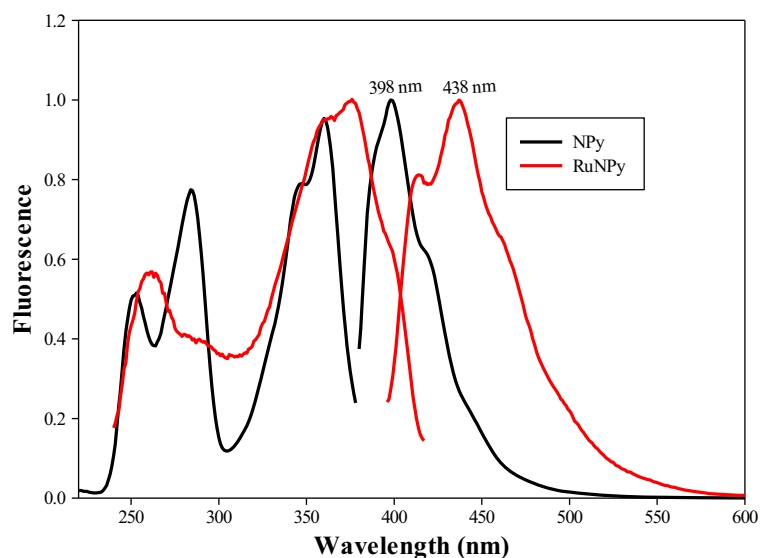
Interestingly, whereas the overall profiles look similar between these two samples, the emission and excitation maxima of RuNC12 exhibit a clear red-shift as compared to those of the monomeric ligands. For instance, the major excitation and emission peaks of NC12 monomers can be identified at 360 and 398 nm, respectively, but they appear at much longer wavelengths of 376 and 438 nm for RuNC12. This is likely due to intraparticle charge delocalization between the particle-bound pyrene groups mediated by the conjugated metal-ligand interfacial bonds, as observed previously with nanoparticles functionalized with metal-carbene or vinylidene bonds (Chen et al. 2009).

Similar behaviors are observed when pyrene moieties are bound onto the nanoparticle surface by ruthenium-vinylidene (Ru = C = CH–) linkages, as demonstrated by the comparison between EPy, di-EPy, and RuEPy (Fig. S6). Experimentally, the emission maximum of EPy monomers can be identified at 387 nm, and at somewhat longer wavelength of 395 nm for RuEPy nanoparticles (in comparison, di-EPy exhibits an emission peak at 448 nm due to effective intramolecular conjugation through the diactylene (−C ≡ C–C ≡ C–) bridge) (Hu et al. 2016a; Kang et al. 2012b). The fact that the red-shift (40 nm) of the RuNPy nanoparticle emission, as compared to NPy monomers, was significantly more pronounced than that for RuEPy might suggest better intraparticle charge delocalization mediated by the Ru–N ≡ C interfacial bond than by Ru = C = CH–.

Conclusion

In summary, stable ruthenium nanoparticles were prepared by the self-assembly of nitrile molecules on the nanoparticle surface. ^{1}H NMR and TGA measurements suggested an end-on configuration of the metal-ligand interfacial bonds. Consistent results were obtained in FTIR measurements, in conjunction of ^{15}N isotopic labeling of the nitrile moiety. XPS measurements indicated that the interfacial bonds were likely dominated by back-donation of Ru 3d electrons to the vacant π^* orbital of the nitrile moiety, leading to a marked downshift of the N 1 s binding energy, as compared to the free ligands. Such strong metal-ligand interfacial bonds allowed for effective intraparticle charge delocalization between the particle-bound functional moieties, as

manifested in photoluminescence measurements of pyrene-functionalized ruthenium nanoparticles. These results expand the toolbox for nanoparticle surface functionalization and further highlight the fundamental importance of metal–organic contacts in the manipulation of intraparticle charge transfer and nanoparticle material properties.

Compliance with ethical standards

Conflict of interest   The authors declare that they have no conflict of interest.

References

Chakroune N et al (2005) Acetate- and thiol-capped monodisperse ruthenium nanoparticles: XPS, XAS, and HRTEM studies. Langmuir 21:6788–6796. doi:10.1021/la050706c

Chen SW et al (1998) Gold nanoelectrodes of varied size: transition to molecule-like charging. Science 280:2098–2101. doi:10.1126/science.280.5372.2098

Chen W, Davies JR, Ghosh D, Tong MC, Konopelski JP, Chen SW (2006) Carbene-functionalized ruthenium nanoparticles. Chem Mater 18:5253–5259

Chen W, Chen SW, Ding FZ, Wang HB, Brown LE, Konopelski JP (2008) Nanoparticle-mediated intervalence transfer. J Am Chem Soc 130:12156–12162. doi:10.1021/ja803887b

Chen W, Zuckerman NB, Lewis JW, Konopelski JP, Chen SW (2009) Pyrene-functionalized ruthenium nanoparticles: novel fluorescence characteristics from intraparticle extended conjugation. J Phys Chem C 113:16988–16995. doi:10.1021/jp906874f

Chen W, Zuckerman NB, Kang XW, Ghosh D, Konopelski JP, Chen SW (2010a) Alkyne-protected ruthenium nanoparticles. J Phys Chem C 114:18146–18152. doi:10.1021/jp101053c

Chen W, Zuckerman NB, Konopelski JP, Chen SW (2010b) Pyrene-functionalized ruthenium nanoparticles as effective Chemosensors for Nitroaromatic derivatives. Anal Chem 82:461–465. doi:10.1021/ac902394s

Chen W, Pradhan S, Chen SW (2011) Photoluminescence and conductivity studies of anthracene-functionalized ruthenium nanoparticles. Nanoscale 3:2294–2300. doi:10.1039/c1nr10158g

Downs EL, Tyler DR (2015) Nitrile and cyanohydrin hydration with nanoparticles formed in situ from a platinum dihydride complex. J Inorg Organomet P 25:73–80. doi:10.1007/s10904-014-0079-z

Griffiths P, de Hasseth JA (2007) Fourier Transform Infrared Spectrometry. Wiley-Blackwell

Hostetler MJ et al (1998) Alkanethiolate gold cluster molecules with core diameters from 1.5 to 5.2 nm: Core and monolayer properties as a function of core size. Langmuir 14:17–30

Hu PG, Chen LM, Deming CP, Bonny LW, Lee H-W, Chen SW (2016a) Identification of the formation of metal-vinylidene interfacial bonds of alkyne-capped platinum nanoparticles by isotopic labeling. Chem Commun 52:11631–11633

Hu PG, Chen LM, Kang XW, Chen SW (2016b) Surface functionalization of metal nanoparticles by conjugated metal-ligand interfacial bonds: impacts on intraparticle charge. Transfer Accounts of Chemical Research 49:2251–2260

Kang XW, Chen SW (2012) Electronic conductivity of alkyne-capped ruthenium nanoparticles. Nanoscale 4:4183–4189. doi:10.1039/c2nr30213f

Kang XW, Zuckerman NB, Konopelski JP, Chen SW (2010) Alkyne-stabilized ruthenium nanoparticles: manipulation of intraparticle charge delocalization by nanoparticle charge. States Angewandte Chemie-International Edition 49:9496–9499. doi:10.1002/anie.201004967

Kang XW, Song Y, Chen SW (2012a) Nitrene-functionalized ruthenium nanoparticles. J Mater Chem 22:19250–19257. doi:10.1039/c2jm33783e

Kang XW, Zuckerman NB, Konopelski JP, Chen SW (2012b) Alkyne-functionalized ruthenium nanoparticles: ruthenium-vinylidene bonds at the metal-ligand Interface. J Am Chem Soc 134:1412–1415. doi:10.1021/ja209568v

Kivrak A, Zora M (2007) Efficient one-pot synthesis of cyanoferrocene from ferrocenecarboxaldehyde using NH2OH center dot HCl/KI/ZnO/CH3CN system. J Organomet Chem 692:2346–2349. doi:10.1016/j.jorganchem.2007.02.002

Leow D, Li G, Mei TS, Yu JQ (2012) Activation of remote meta-CH bonds assisted by an end-on template. Nature 486:518–522. doi:10.1038/nature11158

Lu YZ, Chen W (2012) Sub-nanometre sized metal clusters: from synthetic challenges to the unique property discoveries. Chem Soc Rev 41:3594–3623. doi:10.1039/c2cs15325d

Luque R, Clark JH, Yoshida K, Gai PL (2009) Efficient aqueous hydrogenation of biomass platform molecules using supported metal nanoparticles on Starbons (R) Chemical Communications:5305–5307 doi:10.1039/b911877b

Michelin RA, Mozzon M, Bertani R (1996) Reactions of transition metal-coordinated nitriles coordination. Chemistry Reviews 147:299–338

Oranskaya OM, Filimonov VN (1970) Dokl Akad Nauk SSSR 194:140

Oranskaya O, Filimonov VN, Shmuliakovskii Y A. (1970a) Kinet Katal 11:727

Oranskaya OM, Filimonov VN, Shmuliakovskii YA (1970b) Kinet Katal 11:1289

Oranskaya OM, Semenskaya IV, Filimonov VN (1976) Infrared study of the bonding of adsorbed nitriles to metals reaction kinetics and catalysis. Letters 5:135–139

Roev LM, Filimonov VN, Terenin AN (1958) Opt Spektrosk 4:328

Shanahan KL, Muettertiest EL (1984) Surface coordination chemistry of ruthenium: a survey of ruthenium (001) surface chemistry. J Phys Chem 88:1996–2003

Steiner UB, Caseri WR, Suter UW (1992) Adsorption of Alkanenitriles and Alkanedinitriles on gold and copper. Langmuir 8:2771–2777

Tretyakov NE, Filimonov VN (1973) Kinet Katal 14:803

Uptmoor AC, Freudenberg J, Schwabel ST, Paulus F, Rominger F, Hinkel F, Bunz UHF (2015) Reverse engineering of conjugated microporous polymers: defect structures of Tetrakis (4-ethynylphenyl) stannane. Networks Angewandte Chemie-International Edition 54:14673–14676. doi:10.1002/anie.201506905

Yin WY, He C, Chen M, Zhang H, Lei AW (2009) Nickel-catalyzed oxidative coupling reactions of two different terminal alkynes using O2 as the oxidant at room temperature: facile syntheses of Unsymmetric 1,3-Diynes. Org Lett 11:709–712. doi:10.1021/ol8027863

Zhao ZH, Liu H, Chen SW (2012) Charge transport at the metal oxide and organic interface. Nanoscale 4:7301–7308. doi:10.1039/c2nr32216a